

# Robust Classification by Coupling Data Mollification with Label Smoothing

Markus Heinonen

Department of Computer Science  
Aalto University, Finland

Michael Kampffmeyer

Department of Physics and Technology  
UiT The Arctic University of Norway, Norway

## Abstract

Introducing training-time augmentations is a key technique to enhance generalization and prepare deep neural networks against test-time corruptions. Inspired by the success of generative diffusion models, we propose a novel approach of coupling data mollification, in the form of image noising and blurring, with label smoothing to align predicted label confidences with image degradation. The method is simple to implement, introduces negligible overheads, and can be combined with existing augmentations. We demonstrate improved robustness and uncertainty quantification on the corrupted image benchmarks of the CIFAR and TinyImageNet datasets.

## 1 INTRODUCTION

Image classification is a fundamental task in deep learning that has enjoyed a lot of developments throughout the last decade, while continuing to attract attention thanks to contributions in, e.g., tuning training protocols (Hendrycks et al., 2020; Wightman et al., 2021) and representation learning (Radford et al., 2021). Training-time *augmentations*, whereby models are exposed to input variations to accelerate training (CutMix, MixUp) (Zhang et al., 2018; Yun et al., 2019), mimic test time variability (AugMix, TrivialAugment) (Hendrycks et al., 2020; Müller and Hutter, 2021), or induce robustness against spurious signal (PixMix) (Hendrycks et al., 2022) also represent a rich family of works in this

Ba-Hien Tran

Mathematical and Algorithmic Sciences Lab  
Huawei Paris Research Center, France

Maurizio Filippone

Statistics Program  
KAUST, Saudi Arabia

literature. These approaches result in improvements on test accuracy (Vryniotis, 2021) and on corrupted out-of-distribution test images (Hendrycks and Dietterich, 2019). Somewhat surprisingly, augmentations typically assume that the labels are not degraded, even if an augmentation leads to object occlusion. In a parallel line of work on label smoothing, training labels are decreased to reduce network over-confidence (Szegedy et al., 2016; Müller et al., 2019) with calibration improvements (Guo et al., 2017).

In this paper, we propose a novel approach to improve robustness of classification models to input corruptions by taking inspiration from the literature on Generative Diffusion Models (GDMs) (Song et al., 2021), which are currently dominating the state-of-the-art. A key feature of GDMs is the mechanism of *data mollification* obtained by corrupting inputs by adding noise (Song et al., 2021) or removing signal (Hoogeboom and Salimans, 2023). Recently, Tran et al. (2023) provided evidence that data mollification is responsible for dramatic improvements in density estimation and quality of generated samples in likelihood-based generative models. In this work, we aim to leverage such a key component behind the success of GDMs to improve performance and robustness of classifiers. In our proposal, data mollification in classification materializes in the coupling of *training-time input mollification*, in the form of noising and blurring, with *training-time label mollification* in the form of label smoothing (Szegedy et al., 2016). Label smoothing decreases label confidence based on the intensity of corruption of the inputs (see Fig. 1), which encourages the network to match the predicted label confidence to the amount of noise in the input image.

Our contributions are: (1) We present image classification by training under mollified inputs and labels, and discuss connections to Dirichlet distributions and tempering; (2) We provide a probabilistic view

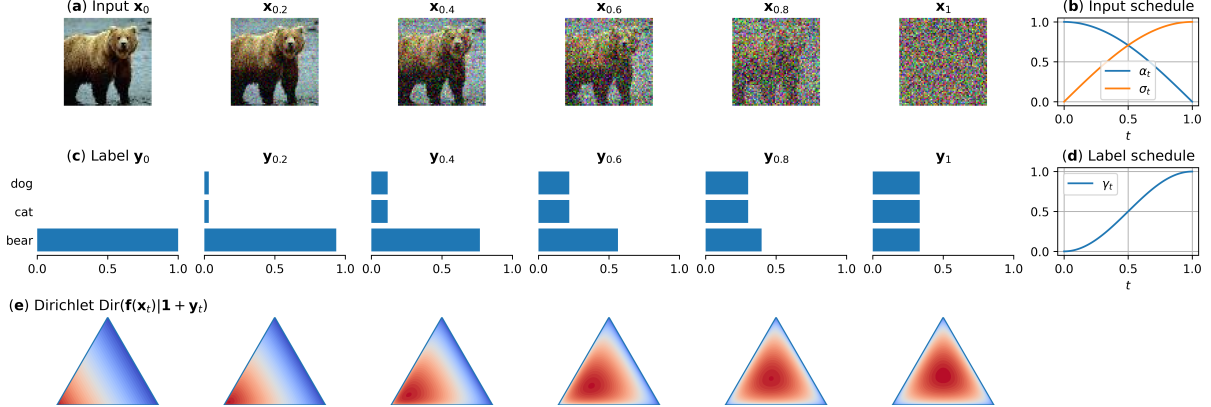


Figure 1: **Mollification augments training with perturbed images (a) and smoothed labels (c).** Input mollification and label smoothing follow monotonic schedules (d), which reflect the signal-to-noise ratio of the images (b). Label smoothing prefers predictions whose distribution matches label uncertainty (e). The method extends to an arbitrary number of classes.

of data mollification and label smoothing, which is simple to implement and can be combined with existing augmentation techniques to improve performance on test-time corrupted images; **(3)** We demonstrate that our approach allows for a better calibration on in-distribution CIFAR-10/100, and TinyImageNet, while yielding strong performance on out-of-distribution data (e.g., sub-10% error rate on CIFAR-10-C).

## 2 RELATED WORKS

**Data Augmentation.** In contrast to earlier works focusing on removing patches from images (see, e.g., [DeVries and Taylor \(2017\)](#)), recent works provide evidence of improving performance of CNNs, by mixing input images in various ways. One of the earliest attempts is MixUp ([Zhang et al., 2018](#)), which fuses pairs of input images and corresponding labels via convex combinations. [Teney et al. \(2024\)](#) and [Yao et al. \(2022\)](#) improved out-of-distribution robustness of MixUp by selectively choosing pairs of inputs using a predefined criterion. Later, CutMix ([Yun et al., 2019](#)) copies and pastes patches of images onto other input images to create collage training inputs. More recently, AugMix ([Hendrycks et al., 2020](#)) proposed mixing multiple naturalistic transformations from AutoAug ([Cubuk et al., 2019](#)), while maintaining augmentation consistency. [Müller and Hutter \(2021\)](#) further proposed TrivialAug where augmentation type and strength are sampled at random. In other approaches, which we consider orthogonal to our work due to their complexity or focus on test-time augmentations, we should mention DeepAugment ([Hendrycks et al., 2021](#)) which uses an additional network to generate augmented data, and [Lee et al. \(2020\)](#) which involves training an ensemble of neural networks. [Schneider et al. \(2020\)](#) and

[Zhang et al. \(2022\)](#) adapt to test-time covariate shifts by modulating the statistics of batch-norm layers or by performing ensemble prediction of a test-image under all possible corruptions.

**Label Smoothing.** Label smoothing ([Szegedy et al., 2016](#)) has been proposed to improve robustness of neural networks when employing data augmentation. For any input image, reusing the same label for the derived augmented images during training induces overconfidence in predictions. Label smoothing addresses this problem by mixing the one-hot label with a uniform distribution while still using the popular cross-entropy loss. This simple modification has been shown to yield better calibrated predictions and uncertainties ([Müller et al., 2019; Thulasidasan et al., 2019](#)). The main question is how to optimally mix the one-hot encoded label with a distribution over the other classes ([Kirichenko et al., 2023](#)), and recent works propose ways to do so by looking at the confidence in predictions over augmented data ([Maher and Kull, 2021; Qin et al., 2023](#)) or relative positioning with respect to the classification decision boundary ([Li et al., 2020](#)).

**Probabilistic perspectives.** Perturbed inputs have been argued to yield degenerate ([Izmailov et al., 2021](#)) or tempered likelihoods ([Kapoor et al., 2022](#)). Several works study how label smoothing mitigates issues with the so-called cold-posterior effect ([Wenzel et al., 2020; Bachmann et al., 2022](#)). [Nabarro et al. \(2022\)](#) proposes an integral likelihood similar to our approach, and applies Jensen lower bound approximation. [Kapoor et al. \(2022\)](#) interprets augmentations and label degradation through a Dirichlet likelihood, and analyze the resulting biases. The work in [Wang et al. \(2023\)](#) considers neural networks with stochastic output layers, which

allows them to cast data augmentation within a formulation involving auxiliary variables. Interestingly, this yields a maximum-a-posteriori (MAP) objective in the form of a logarithm of an expectation, which is optimized via expectation maximization. [Lienen and Hüllermeier \(2021\)](#) propose label relaxation as an alternative to label smoothing by operating with upper bounds on probabilities of class labels. Recently, [Wu and A Williamson \(2024\)](#) use MixUp data augmentation to draw samples from the martingale posterior ([Fong et al., 2023](#)) of neural networks.

### 3 ROBUST CLASSIFICATION THROUGH MOLLIFICATION

We consider supervised machine learning problems with  $N$  observed inputs  $\mathbf{x}$  and labels  $\mathbf{y}$  so that  $\mathcal{D} = (\mathbf{x}_n, \mathbf{y}_n)_{n=1}^N$ , where labels are one-hot-encoded vectors  $\mathbf{y} \in [0, 1]^C$  over  $C$  classes. We focus on image classification problems, which pose a challenge due to their large dimensionality and the need for robustness.

We pose a question inspired by the success of Generative Diffusion Models ([Ho et al., 2020; Song et al., 2021](#)):

*Can we leverage the features that make GDMs so successful in generative modeling and density estimation to obtain classifiers  $p(\mathbf{y}|\mathbf{x})$  that perform well on in-distribution inputs while being robust on out-of-distribution inputs?*

In the GDM literature, tangential discussions around this question have arisen by either adding a classifier on top of the generative model, or carving out the predictive conditionals  $p(\mathbf{y}|\mathbf{x})$  from the generative joint distribution ([Ho and Salimans, 2021; Li et al., 2023](#)). Our goal, instead, is to exploit the mechanism of *data mollification* which characterizes GDMs for the predictive task directly, without building costly GDMs.

In GDMs, the data distribution  $p_0(\mathbf{x}) := p(\mathbf{x})$  is successively annealed into more noisy versions  $p_t(\mathbf{x})$  for  $t \in [0, 1]$  until  $p_1(\mathbf{x}) \sim \mathcal{N}(0, I)$  is pure noise. In image classification, where we aim to estimate a decision boundary among classes, we can follow the same principle and assume a noisy image distribution  $p_t(\mathbf{x}_t|\mathbf{x})$ .

*How should we choose the label distribution of  $\mathbf{y}_t$  given the true label  $\mathbf{y}$  and the noisy image  $\mathbf{x}_t$ ?*

In the extreme  $\mathbf{x}_1 = \epsilon$  the input is pure noise, and the original label surely loses its validity. Therefore, we argue that we need to monotonically degrade the label while noising the input. Similar considerations can be made for input mollification based on blurring.

In this section, we formulate and analyze these concepts,

and show that the application of input mollification and label smoothing to classification can be viewed through the lens of *augmentations*, while in the experiments we demonstrate that this enables significant improvements in predictive performance under corruptions.

#### 3.1 Augmented likelihood

The standard likelihood of a product of pointwise likelihoods stems from De Finetti's theorem ([Cifarelli and Regazzini, 1996](#)) and from i.i.d. data sampling assumption  $\{\mathbf{x}_n, \mathbf{y}_n\} \stackrel{\text{iid}}{\sim} p(\mathbf{x}, \mathbf{y})$ ,

$$\log p(\mathcal{D}|\theta) = \sum_{n=1}^N \log p(\mathbf{y}_n|\mathbf{x}_n, \theta), \quad (1)$$

where  $\theta$  denote model parameters.

We can introduce transformations  $T_\phi(\mathbf{x})$  whose parameters  $\phi$  are auxiliary variables that are marginalized out as follows

$$\mathcal{L} = \log p(\mathcal{D}|\theta) = \sum_{n=1}^N \log \int p(\mathbf{y}_n|\mathbf{x}_n, \phi, \theta) p(\phi) d\phi, \quad (2)$$

where we assume that the prior over the transformations is independent on inputs  $\mathbf{x}_n$  and parameters  $\theta$ . The expression in [Eq. 17](#) gives rise to two main questions:

*How can we efficiently deal with the log-expectation in [Eq. 17](#) to optimize  $\theta$  under input mollification?*

Each likelihood term in [Eq. 17](#) is an expectation under the distribution over transformations, and as such its log-sum form cannot be easily estimated unbiasedly using mini-batches of corrupted inputs. A simple and effective solution is to use Jensen's inequality to obtain a lower bound:

$$\mathcal{L} \geq \sum_{n=1}^N \int \log p(\mathbf{y}_n|\mathbf{x}_n, \phi, \theta) p(\phi) d\phi. \quad (3)$$

Each integral can then be approximated in an unbiased fashion with Monte Carlo by sampling corruption intensities from  $p(\phi)$ , while the sum over  $N$  can also be approximated unbiasedly through mini-batching; this leads to the possibility to obtain stochastic gradients to optimize  $\theta$ .

The second question question is now:

*What form should we choose for  $p(\mathbf{y}_n|\mathbf{x}_n, \phi, \theta)$ ?*

Arguably, *any* image transformation has a probability to degrade its associated label, since it is difficult to think that transformations do not affect label information at all; in an image, transformations such as pixel

noise, crops, zooms or rotations can easily lead to the image losing some of its core meaning. The likelihood  $p(\mathbf{y}_n|\mathbf{x}_n, \phi, \theta)$  should be defined in a way that captures this behavior. We dedicate the rest of this section to an in-depth discussion of how to define a likelihood function for the label associated with corrupted inputs. Before doing so, it is useful to discuss mollification strategies for the inputs, which we do next.

### 3.2 Input Mollification

The two key modalities of input mollification consist of drowning the image in Gaussian noise (Song et al., 2021; Ho et al., 2020), or applying low-pass filters to the image by blurring (Bansal et al., 2024). By repurposing them as training-time augmentations, the model learns to ignore spurious noise patterns, while blur removes textures information and requires the model to perform classification under low-frequency representations of images (Rissanen et al., 2023).

**Noising.** We follow a standard way of mollifying inputs by following the literature on GDMs: (Ho et al., 2020)

$$\mathbf{x}_t^{\text{noise}} = \underbrace{\cos(t\pi/2)}_{\alpha_t} \mathbf{x} + \underbrace{\sin(t\pi/2)}_{\sigma_t} \boldsymbol{\epsilon}, \quad (4)$$

where we mix input image  $\mathbf{x}$  and noise  $\boldsymbol{\epsilon} \sim \mathcal{N}(0, I)$  in proportions of  $\alpha_t$  and  $\sigma_t$  according to the variance-preserving cosine schedule (Nichol and Dhariwal, 2021). We assume the *temperature* parameter  $t \in [0, 1]$  in unit interval. We also assume image standardization to  $\mathbb{E}[\mathbf{x}_n] = 0$  and  $\text{Var}[\mathbf{x}_n] = \mathbf{1}$ .

**Blurring.** We also follow standard practice in blurring for GDMs (Hoogeboom and Salimans, 2023)

$$\mathbf{x}_t^{\text{blur}} = \mathbf{V} \exp(-\tau(t)\mathbf{\Lambda}) \mathbf{V}^T \mathbf{x}, \quad (5)$$

where  $\mathbf{V}^T$  is the discrete cosine transform (DCT),  $\mathbf{\Lambda}$  are the squared frequencies  $[\mathbf{\Lambda}]_{wh} = \pi^2(\frac{w^2}{W^2} + \frac{h^2}{H^2})$  of the pixel coordinates  $(0, 0) \leq (w, h) < (W, H)$ , and  $\tau(t) \geq 0$  is a dissipation time (See Appendix A in Rissanen et al. (2023) for detailed derivations). Blurring corresponds to ‘melting’ the image by a heat equation  $\Delta$  for  $\tau$  time, which is equivalent to convolving the image with a heat kernel of scale  $\sigma_B = \sqrt{2\tau}$  (Rissanen et al., 2023), and we fix dissipation time  $\tau(t) = \sigma_B(t)^2/2$  to the scale. We follow a logarithmic scale between  $\sigma_{\min} = 0.3$  and full image width  $\sigma_{\max} = W$ ,

$$\sigma_B(t) = \exp((1-t)\log\sigma_{\min} + t\log\sigma_{\max}), \quad (6)$$

which has been found to reduce image information linearly (Rissanen et al., 2023). We verify this in Fig. 3,

where we apply the Lempel-Ziv and Huffman compression of PNG codec<sup>1</sup> to blurred TinyImageNet dataset to measure the information content post-blur. See Fig. 2 for blur examples.

### 3.3 Label Smoothing

After discussing possible strategies for mollifying the inputs, we are ready to discuss strategies to define the likelihood function  $p(\mathbf{y}_n|\mathbf{x}_n, \phi, \theta)$  for corrupted inputs. We consider two common forms of label degradation,

$$\mathbf{y}_t^{\text{temp}} = (1 - \gamma_t) \mathbf{y}^{\text{onehot}}, \quad \gamma_t \in [0, 1] \quad (7)$$

$$\mathbf{y}_t^{\text{LS}} = (1 - \gamma_t) \mathbf{y}^{\text{onehot}} + \frac{\gamma_t}{C} \mathbf{1}, \quad (8)$$

where  $\gamma_t : [0, 1] \mapsto [0, 1]$  is a monotonic label decay. The labels  $\mathbf{y}_t$  can be seen to follow a Dirac distribution  $p(\mathbf{y}_t|\mathbf{x}_t, \mathbf{y}) = \delta(\mathbf{y}_t)$ . In the  $\mathbf{y}^{\text{temp}}$  we simply reduce the true label down, while keeping the remaining labels at 0. This has been shown to be equivalent to *tempered* Categorical likelihood (Kapoor et al., 2022)

$$p_{\text{temp}}(\mathbf{y}|\mathbf{f}) = \text{Cat}(\mathbf{y}|\mathbf{f})^{\gamma_t} = f_y^{\gamma_t}. \quad (9)$$

This can be seen as a ‘hot’ tempering as  $\gamma_t < 1$ , where we flatten the likelihood surface.

In contrast, in the  $\mathbf{y}^{\text{LS}}$  we perform *label smoothing*, where we linearly mix one-hot and uniform label vectors (Szegedy et al., 2016; Müller et al., 2019). Label smoothing can seem unintuitive, since we are adding value to all  $C - 1$  incorrect labels. Why should a noisy ‘frog’ image have some ‘airplane’ label?

**Dirichlet interpretation.** To shed light on this phenomenon, we draw a useful interpretation of the Categorical cross-entropy as a Dirichlet distribution

$$\log p(\mathbf{y}|\mathbf{f}) \propto \log \text{Dir}(\mathbf{f}|\mathbf{1} + \mathbf{y}) \quad (10)$$

$$= \sum_c y_c \log f_c - \log B(\mathbf{y}), \quad (11)$$

for a normalized prediction probability vector  $\mathbf{f} = (f_1, \dots, f_C) := \mathbf{f}(\mathbf{x})$ . The Dirichlet distribution is a distribution over normalised probability vectors, which naturally is the probability vector  $\mathbf{f}$ , while the observations are proportional to the class *concentrations* (Sensoy et al., 2018). A higher concentration favors higher probabilities for the respective classes. A standard cross-entropy likelihood for a one-hot label is proportional to Dirichlet with concentrations  $(\dots, 1, 2, 1, \dots)$ .

Fig. 4 compares the Dirichlet densities across clean  $\mathbf{y}^{\text{onehot}}$ , tempered  $\mathbf{y}^{\text{temp}}$  and smoothed  $\mathbf{y}^{\text{LS}}$  labels. We notice that tempering the correct label down flattens

<sup>1</sup>We use `torchvision.io.encode_png`



Figure 2: The logarithmic heat blurring schedule on a TinyImageNet 64×64 image.

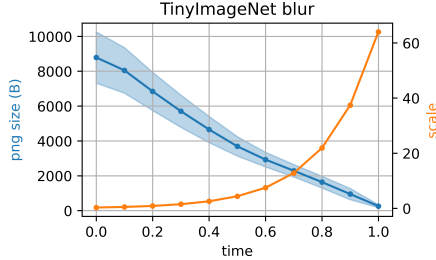


Figure 3: Blur reduces information linearly.

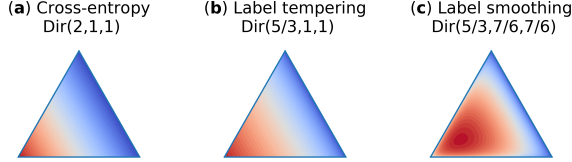


Figure 4: **Label smoothing is an intuitive way to degrade multi-class labels.** The Dirichlet  $\text{Dir}(\mathbf{f}|\mathbf{1} + \mathbf{y})$  visualizations show cross-entropy  $\mathbf{y}^{\text{onehot}}$  (a) and label tempering  $\mathbf{y}^{\text{temp}}$  (b) to retain prediction mode at  $(1, 0, 0)$ , while label smoothing  $\mathbf{y}^{\text{LS}}$  (c) prefers non-peaky predictions.

the slope of the prediction density, but retains its mode at  $\mathbf{f}^* = \mathbf{y}^{\text{onehot}}$ , which can lead to overfitting and poor calibration (Guo et al., 2017) (See Fig. 4c). While increasing the labels of the wrong labels can seem counter-intuitive in label smoothing  $\mathbf{y}^{\text{LS}}$ , it can be shown to favour reduced prediction confidences for corrupted images with a mode  $\mathbf{f}^* = \mathbf{y}^{\text{LS}}$  (See Fig. 4b). The wrong labels are induced to have equal logits.

**Label noising schedule.** Finally, we need to decide how quickly the labels are smoothed given an input  $\mathbf{x}_t$ . For small temperatures (e.g.,  $t < 0.1$ ) we expect close to no effect on the label, while for high temperature (e.g.,  $t > 0.9$ ) we expect the label to almost disappear. For noise-based input mollification, we propose a label decay dependent on the signal-to-noise ratio  $\text{SNR}(t) = \alpha_t^2/\sigma_t^2$  as follows (Kingma et al., 2021):

$$\gamma_t^{\text{noise}} = \left( \frac{1}{1 + \alpha_t^2/\sigma_t^2} \right)^k. \quad (12)$$

That is, when the image has equal amounts of signal and noise with  $\text{SNR}(t) = 1$ , we assume that half of the label remains;  $k$  is a slope hyperparameter, which we estimate empirically.

For blur the SNR is undefined as blurry images contain no added noise. Instead, we propose to apply label smoothing by the number of bits of information in the blurry images, measured through an image compression algorithm. Fig. 3 offers interesting insights on the reduction of information associated with the blurring intensity. Based on this analysis, we define a linear label smoothing approximation

$$\gamma_t^{\text{blur}} = \left( \frac{\text{size}(\mathbf{x}_t.\text{png})}{\text{size}(\mathbf{x}_0.\text{png})} \right)^k \approx t^k, \quad (13)$$

where we apply label smoothing by the bit-ratio, and where  $k$  is a hyperparameter determining either a faster ( $k < 1$ ) or slower ( $k > 1$ ) label decay.

### 3.4 Cross-entropy likelihood

Our analysis points towards label smoothing as a suitable candidate to define a perturbation of the labels associated with mollified inputs, and we propose a cross-entropy-based likelihood

$$\log p(\mathbf{y}|\mathbf{x}, \phi, \theta) = \log p(\mathbf{y}_t^{\text{LS}}|\mathbf{x}_t; \theta) \quad (14)$$

$$= \sum_{c=1}^C \mathbf{y}_{t,c}^{\text{LS}} \log f(\mathbf{x}_t)_c, \quad (15)$$

where  $c$  are the class indices. Using an un-normalised cross-entropy is standard practice in label smoothing (Müller et al., 2019). We note that defining the likelihood with a Dirichlet has a different meaning, since the Dirichlet distribution is normalized such that  $\int \text{Dir}(\mathbf{f}|\mathbf{y}) d\mathbf{f} = 1$ , while a proper likelihood is normalized w.r.t. the data domain  $\mathbf{y}$  (see Kapoor et al. (2022); Wenzel et al. (2020) for a discussion).

## 4 EXPERIMENTS

**Datasets.** We analyze the effect of input mollification and label smoothing, which we collectively refer to as *data mollification*, on the CIFAR-10, CIFAR-100 (Krizhevsky, 2009) and TinyImageNet-200 (Le and Yang, 2015) datasets. The CIFAR datasets contain 50K training images and 10K validation images at  $32 \times 32$  resolution with 10 or 100 classes. The TinyImageNet dataset contains 100K training images with 10K validation images at  $64 \times 64$  resolution over 200 classes. By default we apply training-time augmentations of

Table 1: Results on preactResNet-50 (23.7M params.). FCR: horizontal flips, crops and rotations. A tick mark for ‘‘Moll.’’ indicates the use of the proposed data mollification.

Augmentation	Moll.	CIFAR-10				CIFAR-100				TinyImageNet			
		Error (↓)		NLL (↓)		ECE (↓)		Error		NLL		ECE	
		clean	corr	clean	corr	clean	corr	clean	corr	clean	corr	clean	corr
(none)	✗	11.7	29.2	0.48	1.35	0.09	0.22	39.5	59.9	1.67	2.85	0.15	0.23
FCR	✗	5.0	21.9	0.22	1.26	0.04	0.18	23.2	47.4	0.97	2.30	0.12	0.21
FCR + RandAug	✗	4.4	15.5	0.18	0.75	0.04	0.12	21.5	41.0	0.87	2.09	0.11	0.19
FCR + AutoAug	✗	4.5	13.2	0.19	0.60	0.04	0.10	23.3	39.2	0.93	1.89	0.11	0.18
FCR + AugMix	✗	4.5	10.6	0.18	0.43	0.04	0.08	22.8	35.3	0.94	1.59	0.12	0.16
FCR + TrivAug	✗	<b>3.4</b>	12.1	<b>0.12</b>	0.49	<b>0.03</b>	0.09	20.5	36.9	<b>0.79</b>	1.69	<b>0.10</b>	0.16
FCR + MixUp	✗	4.1	21.9	0.32	0.84	0.19	0.22	21.9	46.1	1.01	2.11	0.18	0.19
FCR + CutMix	✗	4.2	28.4	0.20	1.25	0.09	0.18	22.6	54.2	1.12	2.83	0.18	0.23
(none)	✓	15.8	21.4	0.68	0.87	0.12	0.14	49.3	54.5	2.28	2.53	0.14	0.14
FCR	✓	5.8	10.2	0.25	0.43	0.04	0.08	27.1	34.7	1.17	1.57	0.11	0.13
FCR + RandAug	✓	4.4	8.3	0.18	0.34	0.04	<b>0.07</b>	23.0	30.5	0.96	1.32	<b>0.10</b>	<b>0.12</b>
FCR + AutoAug	✓	4.4	8.2	0.17	<b>0.32</b>	0.04	0.08	23.4	30.6	0.95	1.31	<b>0.10</b>	0.13
FCR + AugMix	✓	5.3	8.6	0.21	0.35	0.04	0.08	25.9	32.5	1.08	1.42	0.11	0.13
FCR + TrivAug	✓	4.0	<b>8.0</b>	0.15	<b>0.32</b>	0.04	<b>0.07</b>	<b>20.4</b>	<b>28.5</b>	0.81	<b>1.19</b>	<b>0.10</b>	<b>0.12</b>
FCR + MixUp	✓	4.7	9.4	0.35	0.51	0.21	0.22	22.5	31.8	1.08	1.47	0.18	0.18
FCR + CutMix	✓	4.1	10.9	0.25	0.47	0.14	0.16	22.6	34.8	1.11	1.65	0.19	0.18

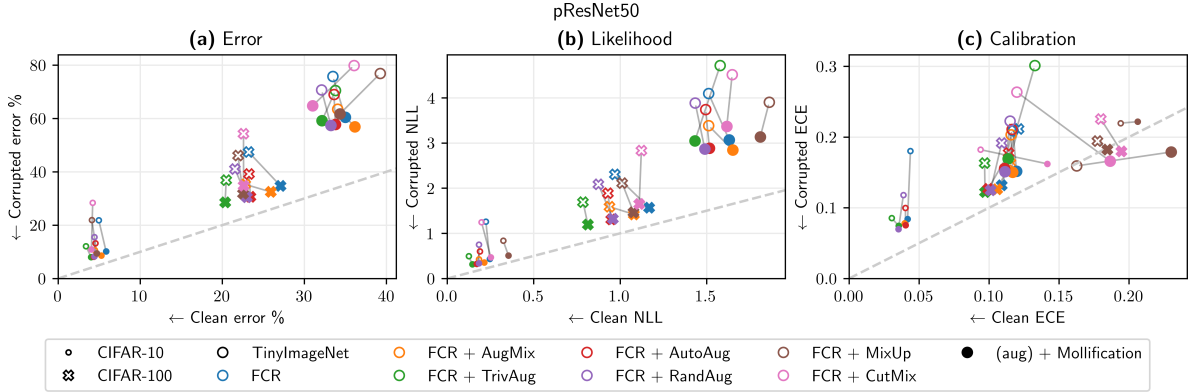


Figure 5: Adding mollification (● ··· ●) to augmentations (○ ··· ○) improves corrupted accuracy (a), likelihood (b) and calibration (c) over CIFAR-10, CIFAR-100 and TinyImageNet.

horizontal flips, random cropping (padding of 4 pixels) and random rotations (up to 15 degrees). We compare six augmentations of AugMix, RandAug, AutoAug, TrivAug, MixUp and CutMix with and without data mollification. We implemented these on PyTorch Lightning, and ran experiments on individual NVIDIA V100 GPUs.

**Training.** We use a preact-ResNet-50 (He et al., 2016) with 23.7 million parameters<sup>2</sup>. We train with SGD for 300 epochs using an initial learning rate of 0.01, which follows a Cosine annealing schedule (Loshchilov and Hutter, 2016). We use mini-batches of size 128, and the cross-entropy-based likelihood. Mollification incurs a negligible running time increase, similar to other augmentations. We find that simple augmentations of flips (F), crops (C) and rotations (R) are always necessary to achieve satisfying performance, even with mollification.

<sup>2</sup>Experiments on other network architectures, such as ResNeXt-29, WRN-40, DenseNet-40 and AllConvNet yielded similar results, and we omit them for clarity.

**Mini-batching.** During training we randomly pick the transformation (noising, blurring, or no mollification) for each image  $\mathbf{x}_n$  in a mini-batch. For the noisy and blurry images we further sample separate temperatures  $t_n \sim \text{Beta}(\alpha, \beta)$  from a Beta distribution per image (see Fig. 7 for an illustration). We choose by default  $\alpha = 1$  and  $\beta = 2$ , which results in average temperature  $\mathbb{E}[t] = 1/3$ .

**Metrics** We report error, negative log-likelihood  $-\log p(\mathbf{y}|\mathbf{f}(\mathbf{x}))$  (NLL), and expected calibration error (ECE) (Guo et al., 2017) on the validation set as well as on corrupted validation images from CIFAR-10-C, CIFAR-100-C and TinyImageNet-C, which contain 75 corruptions of each validation image using 15 types of corruptions at 5 corruption magnitude levels (Hendrycks and Dietterich, 2019). The corruptions di-

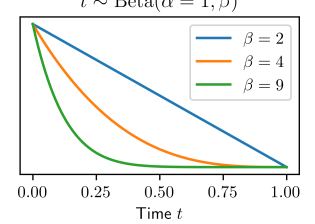


Figure 7: Temperature distributions.

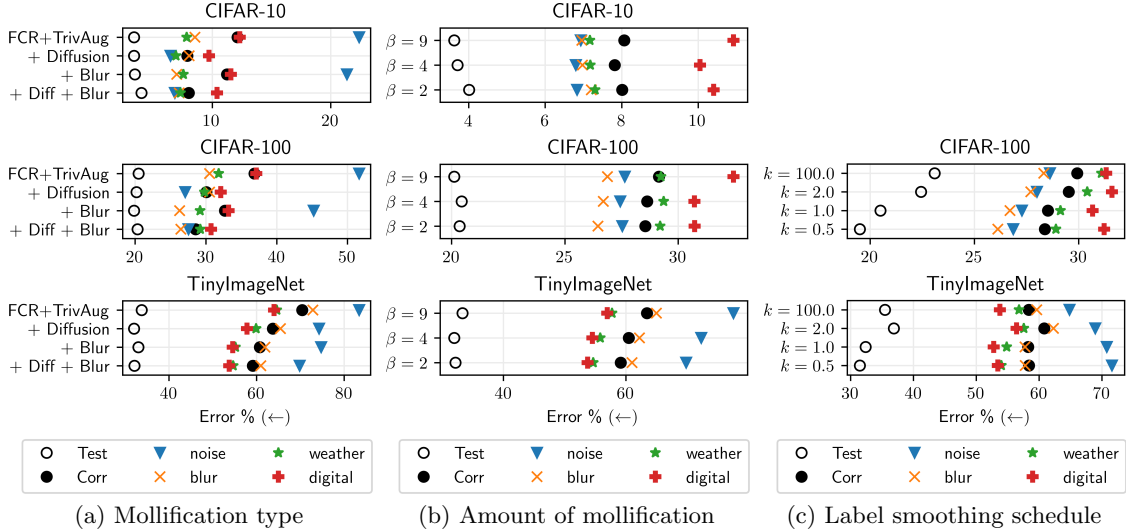


Figure 6: Combining substantial noising and blurring with greedy label smoothing yields good results.

Table 2: Breakdown of errors over individual corruption types for a pResNet-50 network.

		noise			blur				weather				digital				mean	
		Clean	shot	impulse	gauss	motion	zoom	defocus	glass	fog	frost	snow	bright	jpg	pixel	elastic	contrast	
CIFAR10	FCR+TrivAug	<b>3.4</b>	23	13	31	10.0	6.2	5.5	12	<b>6.3</b>	12	9.3	<b>3.9</b>	16	21	7.4	<b>4.4</b>	12
	+ Diffusion	<b>3.4</b>	<b>5.7</b>	<b>7.3</b>	<b>6.4</b>	9.4	6.6	5.8	<b>10</b>	6.8	<b>8.4</b>	<b>8.6</b>	<b>4.0</b>	<b>12</b>	<b>15</b>	7.2	4.9	<b>7.6</b>
	+ Blur	3.5	20	17	27	<b>8.1</b>	<b>4.8</b>	<b>4.1</b>	11	<b>6.4</b>	11	9.2	4.0	17	18	<b>6.5</b>	4.7	11
	+ Diff+Blur	4.0	6.2	7.5	6.8	8.8	5.0	4.6	<b>10</b>	7.1	<b>8.5</b>	9.1	4.5	14	16	6.7	5.3	7.8
CIFAR100	FCR+TrivAug	<b>20</b>	54	39	63	32	28	25	38	30	41	33	23	47	47	30	<b>25</b>	36
	+ Diffusion	<b>20</b>	<b>25</b>	<b>30</b>	<b>26</b>	32	29	27	34	31	34	32	23	<b>37</b>	36	29	26	29
	+ Blur	<b>20</b>	45	40	51	<b>28</b>	<b>23</b>	<b>21</b>	33	<b>29</b>	36	<b>31</b>	<b>22</b>	46	36	<b>26</b>	<b>25</b>	32
	+ Diff+Blur	<b>20</b>	<b>25</b>	31	<b>26</b>	<b>28</b>	23	22	<b>32</b>	30	<b>33</b>	<b>31</b>	23	39	<b>32</b>	27	25	<b>28</b>
TIN	FCR+TrivAug	34	81	85	85	68	71	76	76	65	65	69	60	59	61	61	76	68
	+ Diffusion	<b>32</b>	70	78	75	61	62	68	70	61	60	64	55	52	55	53	71	62
	+ Blur	33	71	77	77	<b>57</b>	58	64	<b>68</b>	<b>56</b>	56	<b>60</b>	<b>50</b>	51	<b>49</b>	<b>49</b>	69	59
	+ Diff+Blur	<b>32</b>	<b>65</b>	<b>73</b>	<b>71</b>	<b>57</b>	<b>57</b>	<b>63</b>	<b>67</b>	<b>56</b>	<b>54</b>	<b>59</b>	<b>50</b>	<b>50</b>	<b>49</b>	<b>49</b>	<b>68</b>	<b>57</b>

vide in four categories of noises (3/15), blurs (4/15), weather effects (3/15), and colorization or compression artifacts (5/15).

#### 4.1 Benchmark results

We report benchmark results in Table 1. We first observe that among the classic augmentation techniques TrivAug combined with FCR is superior with errors of 3.4%, 20.5% and 33.8% in CIFAR-10, CIFAR-100 and TinyImageNet, respectively. Notably, we struggled to achieve good performance with MixUp and CutMix.

When we include mollification, we again observe that TrivAug+Mollification yields highest performance, while mollification improves corrupted image errors on all 6 augmentations on all datasets. On CIFAR-10 we improve corrupted error 12.1%  $\rightarrow$  8.0%, on CIFAR-100 36.9%  $\rightarrow$  28.5% and on TinyImageNet 70%  $\rightarrow$  59%. Mollification also improves the clean performance on the larger TinyImageNet (33.8%  $\rightarrow$  32.2%), has little effect on CIFAR-100, and slightly decreases on CIFAR-10. We also observe minor calibration improvements

from mollification on clean images, while there are some 20% to 40% improvements on calibration on corrupted validation sets.

Fig. 5 shows the relationship between performance on the clean and corrupted validation sets, and it indicates that mollification consistently narrows the gap between clean and corrupted metrics on all datasets. Although our method may in some cases slightly degrade the accuracy on clean data, it consistently and greatly enhances robustness against corruptions and improves uncertainty estimates in most cases, as evidenced by improved performance in terms of NLL and ECE.

We observe that blurring works better on higher-resolution data like TinyImageNet, but it is less effective than noisy augmentation for lower-resolution data like CIFAR-10. We attribute this to CIFAR-10 already being rather down-scaled so that blurring removes label information quickly. In contrast, TinyImageNet images can handle higher blur intensities while retaining label information. A potential future work is to explore resolution-based blur and label smoothing schedules.

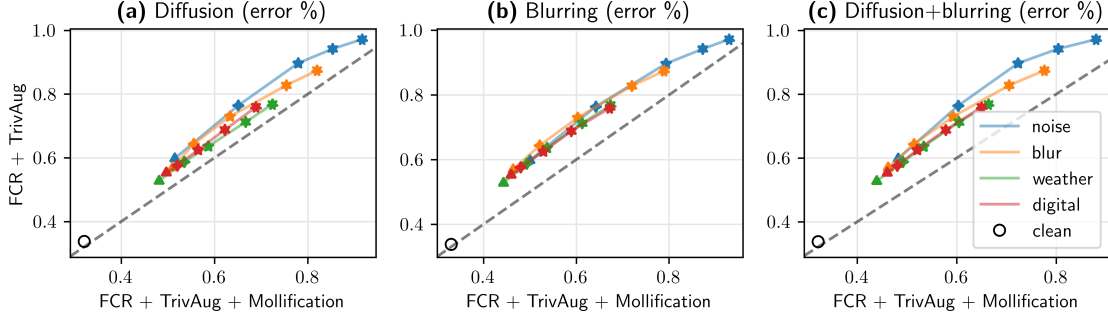


Figure 8: Blurring-based input mollification improves error against all corruption types evenly, while incorporating noise-based mollification adds slight benefits. Polygon size indicates corruption severity from triangles (1) to heptagons (5); experiment on TinyImageNet.

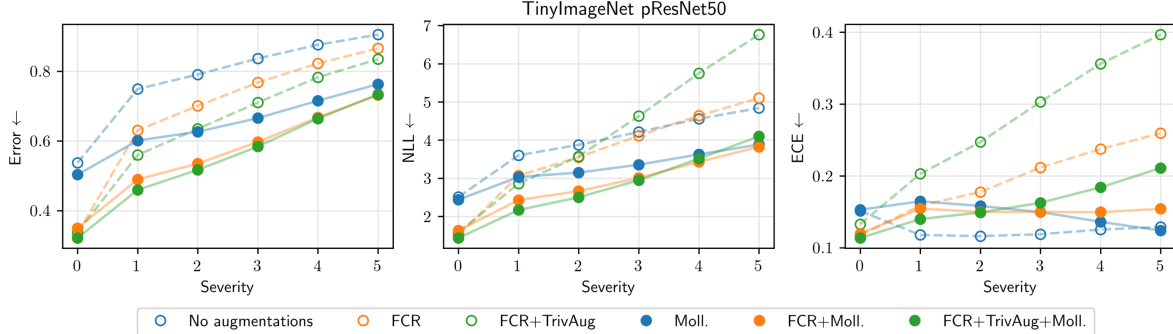


Figure 9: Data mollification improves augmented models over the corruption severity.

#### 4.2 Ablation: How to choose mollification and its intensity?

Next, we study the hyperparameters governing mollification. Fig. 6(a) shows that on smaller CIFAR images noise diffusion improves more than blurring, while on larger TinyImageNet blurring is more advantageous (see Fig. 8). Combining both modes during training is superior in all cases. Notably, training under blur also improves robustness to test noising on TinyImageNet. We also observe that mollification gives highest performance improvements to ‘weather’ and ‘digital’ test corruptions, despite not encoding for them during training time. Fig. 6(b) shows that larger mollification amounts (with  $\beta = 2$ ) gives the best performance, while panel Fig. 6(b) shows the benefits in choosing more aggressive label decay with  $k \leq 1$ .

#### 4.3 Effect of corruption severity

We visualize the performance w.r.t. corruption severity in Fig. 9 for the FCR + TrivAug base augmentation, for which higher values result in higher errors. The mollified versions are in almost all cases better than the corresponding non-mollified ones on all corruption intensities, while giving similar performance on clean images (zero severity).

#### 4.4 Which corruptions do we improve?

The corruptions in the corrupted datasets fall into four categories. Fig. 6 shows a general trend of the network being most robust against ‘digital’ and ‘weather’ corruptions, while ‘blur’ corruptions are moderately difficult, and ‘noise’ corruptions are most difficult to predict correctly. In the Appendix, we provide a spectral analysis explanation for this phenomenon. Table 2 shows the performance w.r.t. the 15 individual corruptions over the three datasets. Mollification improves consistently: in TinyImageNet all individual corruption types improve between 9 and 16 percentage points from TrivAug, which is the best performing conventional augmentation method.

## 5 CONCLUSIONS

We proposed data mollification for supervised image recognition by coupling input mollification and label smoothing to enhance robustness against test-time corruptions. Our work provides a probabilistic interpretation of data mollification and draws connections with augmentations. An interesting future work lies in class-specific noising structures, as well as on analyzing adversarial robustness. Another future research line is to formally connect mollification with regularization.

There are two additional aspects where we hoped our work could give some breakthrough. **(1)** We lower bound the augmented likelihood in Eq. 17 through Jensen’s inequality, similarly to Wenzel et al. (2020). We attempted an unbiased correction of the log expectation using ideas from Durbin and Koopman (1997). **(2)** We employ a likelihood derived from the cross-entropy loss (Eq. 14) and we were able to derive a normalization of this improper likelihood when labels are continuous in  $[0, 1]$ . Surprisingly, none of these ways to recover a proper treatment of the likelihood led to improvements, while complicating the implementation and the numerical stability of the training (see derivations in the Appendix).

## References

G. Bachmann, L. Noci, and T. Hofmann. How tempering fixes data augmentation in Bayesian neural networks. In *ICML*, 2022.

A. Bansal, E. Borgnia, H.-M. Chu, J. Li, H. Kazemi, F. Huang, M. Goldblum, J. Geiping, and T. Goldstein. Cold diffusion: Inverting arbitrary image transforms without noise. *Advances in Neural Information Processing Systems*, 36, 2024.

Y. Burda, R. Grosse, and R. Salakhutdinov. Importance weighted autoencoders. In *ICLR*, 2016.

D. M. Cifarelli and E. Regazzini. De Finetti’s contribution to probability and statistics. *Statistical Science*, 11(4):253–282, 1996.

E. D. Cubuk, B. Zoph, D. Mané, V. Vasudevan, and Q. V. Le. AutoAugment: Learning augmentation strategies from data. In *CVPR*, 2019.

T. DeVries and G. W. Taylor. Improved regularization of convolutional neural networks with cutout. *arXiv*, 2017.

J. Durbin and S. Koopman. Monte Carlo maximum likelihood estimation for non-Gaussian state space models. *Biometrika*, 1997.

E. Fong, C. Holmes, and S. G. Walker. Martingale posterior distributions. *Journal of the Royal Statistical Society Series B: Statistical Methodology*, 85(5):1357–1391, 2023.

C. Guo, G. Pleiss, Y. Sun, and K. Q. Weinberger. On calibration of modern neural networks. In *ICML*, 2017.

K. He, X. Zhang, S. Ren, and J. Sun. Identity mappings in deep residual networks. In *ECCV*, 2016.

D. Hendrycks and T. Dietterich. Benchmarking neural network robustness to common corruptions and perturbations. In *ICLR*, 2019.

D. Hendrycks, N. Mu, E. D. Cubuk, B. Zoph, J. Gilmer, and B. Lakshminarayanan. Augmix: A simple data processing method to improve robustness and uncertainty. In *ICLR*, 2020.

D. Hendrycks, S. Basart, N. Mu, S. Kadavath, F. Wang, E. Dorundo, R. Desai, T. Zhu, S. Parajuli, M. Guo, et al. The many faces of robustness: A critical analysis of out-of-distribution generalization. In *ICCV*, 2021.

D. Hendrycks, A. Zou, M. Mazeika, L. Tang, B. Li, D. Song, and J. Steinhardt. PixMix: Dreamlike pictures comprehensively improve safety measures. In *CVPR*, 2022.

J. Ho and T. Salimans. Classifier-free diffusion guidance. In *NeurIPS workshop on Deep Generative Models*, 2021.

J. Ho, A. Jain, and P. Abbeel. Denoising diffusion probabilistic models. In *NeurIPS*, 2020.

E. Hoffer, T. Ben-Nun, I. Hubara, N. Giladi, T. Hoefler, and D. Soudry. Augment your batch: Improving generalization through instance repetition. In *CVPR*, 2020.

E. Hoogeboom and T. Salimans. Blurring diffusion models. In *ICLR*, 2023.

P. Izmailov, S. Vikram, M. D. Hoffman, and A. G. Wilson. What are bayesian neural network posteriors really like? In *ICML*, 2021.

S. Kapoor, W. Maddox, P. Izmailov, and A. G. Wilson. On uncertainty, tempering, and data augmentation in bayesian classification. In *NeurIPS*, 2022.

D. Kingma, T. Salimans, B. Poole, and J. Ho. Variational diffusion models. In *NeurIPS*, 2021.

P. Kirichenko, M. Ibrahim, R. Balestriero, D. Bouchacourt, R. Vedantam, H. Firooz, and A. G. Wilson. Understanding the detrimental class-level effects of data augmentation. In *NeurIPS*, 2023.

A. Krizhevsky. Learning multiple layers of features from tiny images. Technical report, 2009.

Y. Le and X. S. Yang. Tiny ImageNet visual recognition challenge. 2015.

J. Lee, T. Won, T. K. Lee, H. Lee, G. Gu, and K. Hong. Compounding the performance improvements of assembled techniques in a convolutional neural network. *arXiv*, 2020.

A. C. Li, M. Prabhudesai, S. Duggal, E. Brown, and D. Pathak. Your diffusion model is secretly a zero-shot classifier. In *ICCV*, 2023.

W. Li, G. Dasarathy, and V. Berisha. Regularization via structural label smoothing. In *AISTATS*, 2020.

J. Lienen and E. Hüllermeier. From label smoothing to label relaxation. In *AAAI*, 2021.

I. Loshchilov and F. Hutter. Sgdr: Stochastic gradient descent with warm restarts. In *ICLR*, 2016.

Y. Luo, A. Beatson, M. Norouzi, J. Zhu, D. Duvenaud, R. P. Adams, and R. T. Chen. Sumo: Unbiased estimation of log marginal probability for latent variable models. In *ICLR*, 2020.

M. Maher and M. Kull. Instance-based label smoothing for better calibrated classification networks. In *ICMLA*, 2021.

R. Müller, S. Kornblith, and G. E. Hinton. When does label smoothing help? In *NeurIPS*, 2019.

S. G. Müller and F. Hutter. Trivialaugment: Tuning-free yet state-of-the-art data augmentation. In *ICCV*, 2021.

S. Nabarro, S. Ganev, A. Garriga-Alonso, V. Fortuin, M. van der Wilk, and L. Aitchison. Data augmentation in bayesian neural networks and the cold posterior effect. In *UAI*, 2022.

A. Nichol and P. Dhariwal. Improved denoising diffusion probabilistic models. In *ICML*, 2021.

Y. Qin, X. Wang, B. Lakshminarayanan, E. H. Chi, and A. Beutel. What are effective labels for augmented data? improving calibration and robustness with AutoLabel. In *IEEE Conference on Secure and Trustworthy Machine Learning*, 2023.

A. Radford, J. W. Kim, C. Hallacy, A. Ramesh, G. Goh, S. Agarwal, G. Sastry, A. Askell, P. Mishkin, J. Clark, et al. Learning transferable visual models from natural language supervision. In *ICML*, 2021.

S. Rissanen, M. Heinonen, and A. Solin. Generative modelling with inverse heat dissipation. In *ICLR*, 2023.

S. Schneider, E. Rusak, L. Eck, O. Bringmann, W. Brendel, and M. Bethge. Improving robustness against common corruptions by covariate shift adaptation. 2020.

M. Sensoy, L. Kaplan, and M. Kandemir. Evidential deep learning to quantify classification uncertainty. In *NeurIPS*, 2018.

N. Shephard and M. Pitt. Likelihood analysis of non-gaussian measurement time series. *Biometrika*, 1997.

Y. Song, J. Sohl-Dickstein, D. P. Kingma, A. Kumar, S. Ermon, and B. Poole. Score-based generative modeling through stochastic differential equations. In *ICLR*, 2021.

C. Szegedy, V. Vanhoucke, S. Ioffe, J. Shlens, and Z. Wojna. Rethinking the inception architecture for computer vision. In *CVPR*, 2016.

D. Teney, J. Wang, and E. Abbasnejad. Selective mixup helps with distribution shifts, but not (only) because of mixup. In *ICML*, 2024.

S. Thulasidasan, G. Chennupati, J. A. Bilmes, T. Bhattacharya, and S. Michalak. On mixup training: Improved calibration and predictive uncertainty for deep neural networks. In *NeurIPS*, 2019.

B.-H. Tran, G. Franzese, P. Michiardi, and M. Filippone. One-line-of-code data mollification improves optimization of likelihood-based generative models. In *NeurIPS*, 2023.

V. Vryniotis. How to Train State-Of-The-Art Models Using TorchVision’s Latest Primitives. [pytorch.org](https://pytorch.org), 2021.

Y. Wang, N. Polson, and V. O. Sokolov. Data Augmentation for Bayesian Deep Learning. *Bayesian Analysis*, 2023.

F. Wenzel, K. Roth, B. Veeling, J. Swiatkowski, L. Tran, S. Mandt, J. Snoek, T. Salimans, R. Jenatton, and S. Nowozin. How good is the Bayes posterior in deep neural networks really? In *ICML*, 2020.

R. Wightman, H. Touvron, and H. Jégou. Resnet strikes back: An improved training procedure in timm. In *NeurIPS workshop on ImageNet PPF*, 2021.

L. Wu and S. A. Williamson. Posterior uncertainty quantification in neural networks using data augmentation. In *AISTATS*, 2024.

H. Yao, Y. Wang, S. Li, L. Zhang, W. Liang, J. Zou, and C. Finn. Improving out-of-distribution robustness via selective augmentation. In *ICML*, 2022.

S. Yun, D. Han, S. J. Oh, S. Chun, J. Choe, and Y. Yoo. Cutmix: Regularization strategy to train strong classifiers with localizable features. In *ICCV*, 2019.

H. Zhang, M. Cisse, Y. N. Dauphin, and D. Lopez-Paz. mixup: Beyond empirical risk minimization. In *ICLR*, 2018.

M. Zhang, S. Levine, and C. Finn. Memo: Test time robustness via adaptation and augmentation. 2022.

## A ADDITIONAL RESULTS

### A.1 Results on ImageNet

We tested the proposed mollification approach based on input mollification and label smoothing on ImageNet. Due to the large size of this dataset, we decided to perform a variation on the experimental setup considered in the main paper. In particular, we consider a pretrained ResNet50 architecture and we fine-tune it for 10 epochs instead of training the model from scratch. In addition, we focus on the following augmentations: AutoAug, AugMix, TrivAug, MixUp and CutMix, which are the ones that performed best on the other datasets, as reported in the main paper.

Table 3: Results on ImageNet with a ResNet-50 architecture. FCR: horizontal flips, crops and rotations. A tick mark for “Moll.” indicates the use of the proposed data mollification.

Augmentation	Moll.	ImageNet							
		Error (↓)		NLL (↓)		ECE (↓)		clean	corr
		clean	corr	clean	corr	clean	corr		
(none)	✗	24.1	63.3	0.93	3.59	0.10	0.17		
FCR	✗	24.7	62.9	0.97	3.56	0.10	0.18		
FCR + RandAug	✗	25.1	60.3	0.98	3.26	0.11	0.17		
FCR + AutoAug	✗	25.5	60.0	1.00	3.19	0.10	0.16		
FCR + AugMix	✗	25.5	60.8	0.99	3.31	0.10	0.17		
FCR + TrivAug	✗	25.3	58.9	0.98	3.11	0.11	0.16		
FCR + MixUp	✗	27.5	63.1	1.36	3.50	0.22	0.16		
FCR + CutMix	✗	25.6	63.6	1.19	3.51	0.18	0.15		
(none)	✓	25.0	56.8	1.00	3.23	0.11	0.20		
FCR	✓	25.8	55.8	1.04	3.06	0.11	0.18		
FCR + RandAug	✓	26.2	54.3	1.05	2.98	0.11	0.19		
FCR + AutoAug	✓	26.6	54.5	1.06	2.96	0.11	0.18		
FCR + AugMix	✓	26.2	53.7	1.04	2.88	0.11	0.18		
FCR + TrivAug	✓	26.2	53.2	1.05	2.87	0.11	0.18		
FCR + MixUp	✓	27.6	54.9	1.33	3.05	0.20	0.21		
FCR + CutMix	✓	26.8	56.3	1.26	3.16	0.19	0.20		

In [Table 3](#), we report performance metrics on clean validation images and on the collective of all corrupted validation images from the ImageNet-C collection; the error metrics are averaged across all 15 corruption types and 5 intensity levels. We report a breakdown of the error metrics ImageNet-C validation images in [Table 4](#) as differences between runs with and without mollification so as to highlight the performance gains offered by mollification for individual corruption types.

Table 4: Breakdown of errors over individual corruption types for a ResNet-50 network on ImageNet. The numbers in the table are the differences between the errors obtained with and without mollification, so negative numbers indicate improvements of mollification with respect to baselines without mollification.

Moll.	Clean	noise			blur			weather			digital			mean				
		shot	impulse	gauss	motion	zoom	defocus	glass	fog	frost	snow	bright	jpg	pixel				
ImageNet	(none)	0.9	-26.0	-29.9	-27.2	-2.0	0.1	-12.4	-1.2	-2.6	0.1	1.2	1.2	3.5	0.1	-0.5	-2.2	-6.5
	FCR	1.1	-25.6	-28.5	-26.4	-2.2	-0.3	-17.9	-2.3	-4.3	-0.2	0.9	0.6	3.9	-0.9	-1.4	-3.1	-7.2
	FCR + RandAug	1.1	-20.7	-22.2	-21.7	-2.2	0.0	-18.0	-1.9	-4.1	-0.1	1.0	1.0	2.4	-0.2	-0.8	-2.7	-6.0
	FCR + AutoAug	1.1	-18.7	-19.3	-20.1	-1.1	0.2	-16.3	-1.2	-4.1	-1.3	0.2	0.0	2.8	1.2	-1.3	-3.0	-5.5
	FCR + AugMix	0.7	-22.2	-26.7	-23.9	-2.1	-0.4	-16.7	-2.4	-3.8	-1.1	-0.1	0.1	1.3	-1.4	-2.0	-4.7	-7.1
	FCR + TrivAug	0.9	-20.4	-22.6	-20.9	-2.7	-0.8	-15.6	-1.3	-1.8	-1.4	0.5	0.6	2.3	-0.1	-0.8	-0.2	-5.7
	FCR + MixUp	0.1	-25.5	-27.7	-25.9	-4.0	-2.0	-21.5	-3.5	-4.2	-0.4	0.0	-0.2	0.5	-0.9	-2.8	-4.8	-8.2
	FCR + CutMix	1.1	-27.0	-29.1	-27.7	-2.5	-0.7	-14.5	-1.4	-3.2	-0.6	-0.2	0.7	2.0	-2.8	-1.4	-1.6	-7.3

It is interesting to note that even in the ImageNet dataset, mollification offers a wide range of significant improvements on error rate across all corruption types, at the expense of a small degradation in performance on clean validation images. [Table 4](#) shows that these gains are particularly significant for corruptions in the noise and blur categories, as expected.

It would be interesting to see whether longer running times would further improve these results. It would also be

interesting to replicate the experimental setup of the main paper where models are trained from scratch. However, we are severely limited by the size of this training and validation datasets, which require high-end computing facilities and several hours for training and validation.

## A.2 Result table from the main paper with standard deviations

For completeness, we report Table 1 from the main paper where we add standard deviations for all metrics.

Table 5: Results on CIFAR-10, CIFAR-100, and TinyImageNet with standard deviations in parentheses.

Augmentation	Moll.	CIFAR-10				CIFAR-100				TinyImageNet			
		Error (↓)		NLL (↓)		ECE (↓)		Error		NLL		ECE	
		clean	corr										
presnet50	✗	11.7 (0.10)	29.4 (0.63)	0.49 (0.01)	1.34 (0.04)	0.09 (0.00)	0.22 (0.01)	39.2 (0.40)	60.3 (0.39)	1.64 (0.02)	2.89 (0.06)	0.16 (0.01)	0.24 (0.01)
FCR	✗	4.9 (0.05)	21.2 (1.01)	0.22 (0.00)	1.14 (0.15)	0.04 (0.00)	0.17 (0.01)	23.2 (0.19)	47.1 (0.33)	0.99 (0.01)	2.32 (0.06)	0.12 (0.00)	0.21 (0.01)
FCR+RandAug	✗	4.2 (0.15)	15.2 (0.41)	0.18 (0.00)	0.73 (0.03)	0.04 (0.00)	0.12 (0.05)	21.4 (0.59)	41.4 (0.00)	0.87 (0.07)	2.09 (0.00)	0.11 (0.00)	0.19 (0.00)
FCR+AutoAug	✗	4.6 (0.07)	13.3 (0.47)	0.19 (0.00)	0.60 (0.04)	0.04 (0.00)	0.10 (0.00)	22.7 (0.33)	38.8 (0.36)	0.91 (0.01)	1.86 (0.05)	0.11 (0.00)	0.17 (0.00)
FCR+AugMix	✗	4.4 (0.06)	10.7 (0.26)	0.18 (0.00)	0.43 (0.01)	0.04 (0.00)	0.08 (0.31)	23.0 (0.34)	35.5 (0.02)	0.94 (0.02)	1.60 (0.00)	0.12 (0.00)	0.16 (0.00)
FCR+TrivAug	✗	3.4 (0.02)	12.2 (0.37)	0.12 (0.00)	0.50 (0.02)	0.03 (0.00)	0.09 (0.00)	20.2 (0.17)	36.8 (0.50)	0.78 (0.01)	1.69 (0.05)	0.10 (0.00)	0.16 (0.00)
FCR+MixUp	✗	3.8 (0.17)	21.9 (1.47)	0.29 (0.02)	0.83 (0.04)	0.17 (0.01)	0.20 (0.02)	21.3 (0.49)	45.1 (0.72)	0.96 (0.04)	2.06 (0.06)	0.15 (0.02)	0.18 (0.03)
FCR+CutMix	✗	3.9 (0.17)	28.2 (0.73)	0.22 (0.01)	1.19 (0.11)	0.11 (0.01)	0.19 (0.02)	22.6 (0.05)	54.3 (0.36)	1.12 (0.00)	2.81 (0.11)	0.18 (0.01)	0.22 (0.02)
presnet50	✓	15.3 (0.07)	20.6 (0.21)	0.65 (0.01)	0.83 (0.01)	0.11 (0.00)	0.13 (0.00)	49.5 (0.20)	54.7 (0.17)	2.29 (0.01)	2.54 (0.01)	0.15 (0.00)	0.14 (0.00)
FCR	✓	5.8 (0.17)	10.2 (0.15)	0.24 (0.01)	0.43 (0.01)	0.04 (0.00)	0.08 (0.07)	27.0 (0.19)	34.7 (0.19)	1.16 (0.01)	1.56 (0.01)	0.11 (0.00)	0.13 (0.00)
FCR+RandAug	✓	4.4 (0.06)	8.3 (0.10)	0.18 (0.00)	0.34 (0.01)	0.04 (0.00)	0.07 (0.07)	23.2 (0.18)	30.6 (0.00)	0.96 (0.00)	1.33 (0.01)	0.10 (0.00)	0.13 (0.00)
FCR+AutoAug	✓	4.2 (0.05)	8.2 (0.15)	0.17 (0.00)	0.33 (0.01)	0.04 (0.00)	0.07 (0.12)	23.7 (0.24)	30.8 (0.00)	0.96 (0.00)	1.32 (0.01)	0.10 (0.00)	0.13 (0.00)
FCR+AugMix	✓	5.4 (0.11)	8.7 (0.11)	0.22 (0.00)	0.36 (0.01)	0.04 (0.00)	0.08 (0.30)	25.7 (0.11)	32.3 (0.01)	1.09 (0.01)	1.42 (0.00)	0.10 (0.00)	0.13 (0.00)
FCR+TrivAug	✓	3.7 (0.07)	7.7 (0.33)	0.14 (0.00)	0.30 (0.02)	0.03 (0.00)	0.07 (0.20)	20.5 (0.35)	28.4 (0.01)	0.81 (0.02)	1.19 (0.00)	0.09 (0.00)	0.12 (0.00)
FCR+MixUp	✓	4.5 (0.10)	9.4 (0.22)	0.34 (0.01)	0.50 (0.01)	0.20 (0.01)	0.21 (0.00)	23.3 (0.38)	32.3 (0.30)	1.12 (0.03)	1.51 (0.01)	0.20 (0.00)	0.20 (0.00)
FCR+CutMix	✓	4.0 (0.06)	10.7 (0.24)	0.26 (0.01)	0.48 (0.01)	0.15 (0.00)	0.17 (0.06)	22.5 (0.20)	34.7 (0.03)	1.13 (0.02)	1.66 (0.02)	0.21 (0.01)	0.19 (0.01)

## A.3 Mollification vs severity

In Fig. 10 we provide a breakdown of performance metrics for the corrupted CIFAR-100 and TinyImageNet over corruption severity (zero being clean validation data). It is not surprising that the metrics degrade with intensity of the corruptions. Meanwhile, it is interesting to observe that mollification attenuates this effect less with performance more stable across corruption severities.

## B SPECTRAL ANALYSIS

In Fig. 11 we compute the average discrete cosine transform (DCT) change from corruptions over TinyImageNet validation set ( $N = 10,000$  images  $\mathbf{x}_i$ ),

$$\frac{1}{N} \sum_{i=1}^N \text{abs}(\text{DCT}[\text{corruption}[\mathbf{x}_i]] - \text{DCT}[\mathbf{x}_i]) \quad (16)$$

Fig. 11 shows which frequencies are modulated by each corruption type. Noise corruptions affect all frequencies uniformly, while blur corruptions follow an exponential decay on the frequencies. Weather corruptions affect dominantly the low frequencies (top-left) in blur-like pattern. The set of digital corruptions are divided into noise-like and blur-like frequency modulation, with pixelate being an outlier. This analysis suggests spectral similarities between noise/blur and digital/weather corruptions.

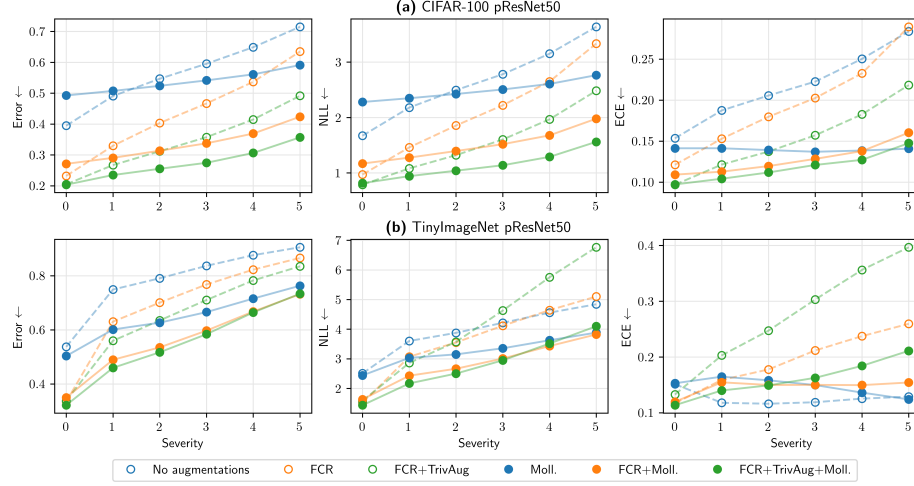


Figure 10: Adding mollification improves augmented models over corruption severity.

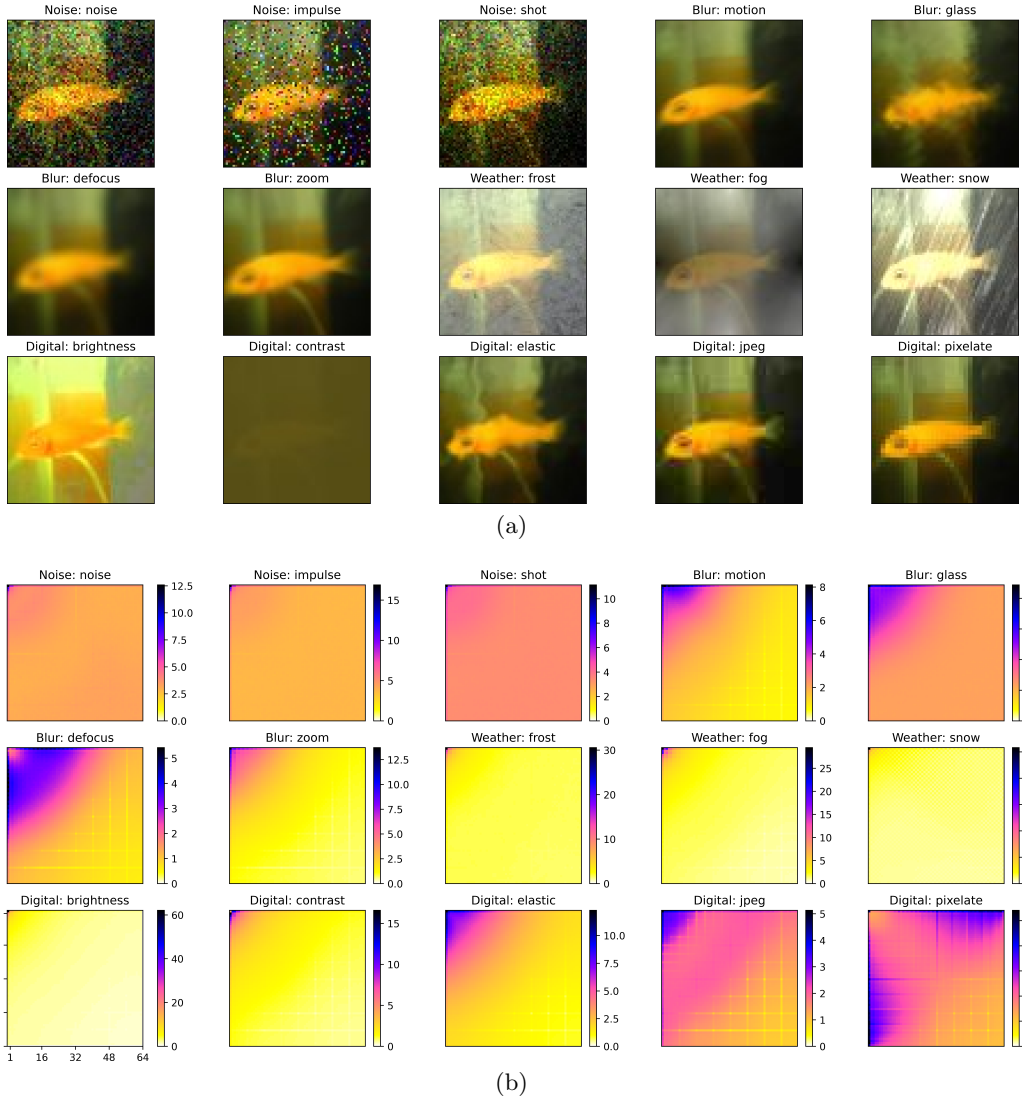


Figure 11: The DCT spectral densities (b) of the 15 corruption types (a). The weather and digital corruptions align resemble the uniform or exponential densities of noise and blur, respectively.

## C NORMALIZING THE CROSS-ENTROPY-BASED LIKELIHOOD

Let's consider label smoothing with soft labels defined as

$$\mathbf{y}^{\text{LS}} = (1 - a)\mathbf{y}^{\text{onehot}} + \frac{a}{C}\mathbf{1},$$

where we have introduced  $a = \gamma_t - 1$ .

We are interested in deriving an expression for a proper cross-entropy-based likelihood function expressing  $p(\mathbf{y}^{\text{LS}}|\mathbf{x}; \theta)$ . In other words, we require that  $p(\mathbf{y}^{\text{LS}}|\mathbf{x}; \theta)$  is indeed a proper distribution over  $\mathbf{y}^{\text{LS}}$ . The difficulty is that the domain of the labels is now continuous and the cross-entropy loss does not correspond to the negative of the logarithm of a properly normalized likelihood.

Soft labels  $\mathbf{y}^{\text{LS}}$  depend on  $a$  and  $\mathbf{y}^{\text{onehot}}$ . For simplicity, let's denote the one-hot vectors  $\mathbf{y}^{\text{onehot}}$  with a one in position  $j$  as  $\mathbf{e}_j$ . With this definition, the normalization constant to obtain a proper likelihood can be expressed as follows:

$$Z = \sum_{j=1}^C \int_0^1 \prod_{i=1}^C f_i^{(\mathbf{y}^{\text{LS}}(a, \mathbf{e}_j))_i} da.$$

Note that  $f_i$  here represent probabilities of class label  $i$ , that is these are the values post-softmax transformation of the output of the network. Without loss of generality, let's focus on the case  $j = 1$ :

$$\int_0^1 \prod_{i=1}^C f_i^{(\mathbf{y}^{\text{LS}}(a, \mathbf{e}_1))_i} da = \int_0^1 f_1^{1-a+\frac{a}{C}} f_2^{\frac{a}{C}} \dots f_C^{\frac{a}{C}} da,$$

which we can simplify into:

$$f_1 \int_0^1 f_1^{a-\frac{1-C}{C}} f_2^{\frac{a}{C}} \dots f_C^{\frac{a}{C}} da = f_1 \int_0^1 \left( f_1^{\frac{1-C}{C}} f_2^{\frac{1}{C}} \dots f_C^{\frac{1}{C}} \right)^a da.$$

We can proceed in a similar way for any  $\mathbf{e}_j$ , and we can compact the expression of the integral further as:

$$f_j \int_0^1 \left( f_j^{-1} \prod_{i=1}^C f_i^{\frac{1}{C}} \right)^a da = f_j \int_0^1 \left( \frac{K}{f_j} \right)^a da,$$

where we have introduced  $K = \prod_{i=1}^C f_i^{\frac{1}{C}}$ .

The normalization constant  $Z$  is the sum over  $j$  of these integrals, for which the solution is in the form:

$$\int_0^1 z^a da = \frac{z-1}{\log z},$$

which yields:

$$Z = \sum_{j=1}^C f_j \int_0^1 \left( \frac{K}{f_j} \right)^a da = \sum_{j=1}^C \frac{K - f_j}{\log(K) - \log(f_j)}.$$

This expression requires some care in the implementation to avoid underflows in extreme cases where one of the  $f_j$  is close to one, and in practice it is better to attempt computing  $\log Z$  instead. We tested the cross-entropy-based likelihood with this normalization, but we did not obtain any improvement in performance while complicating the implementation.

## D UNBIASED ESTIMATE OF THE MARGINAL AUGMENTED LIKELIHOOD

In the main paper, we introduced the marginalized form of the augmented likelihood under transformations  $T_\phi(\mathbf{x})$  of the inputs:

$$\mathcal{L} = \log p(\mathcal{D}|\theta) = \sum_{n=1}^N \log \int p(\mathbf{y}_n|\mathbf{x}_n, \phi, \theta) p(\phi) d\phi, \quad (17)$$

The log-likelihood in Eq. 17 is intractable due to an integral over the space of continuous corruptions or augmentations. Furthermore, simple Monte Carlo averaging of the likelihood within the logarithm is biased for  $K > 1$  (Durbin and Koopman, 1997),

$$\mathcal{L} = \log p(\mathcal{D}|\theta) = \sum_{n=1}^N \log \int p(\mathbf{y}_n|\mathbf{x}_n, \phi; \theta) p(\phi) d\phi \quad (18)$$

$$\approx \sum_{n=1}^N \log \frac{1}{K} \sum_{k=1}^K p(\mathbf{y}_n|\mathbf{x}_n, \phi_k; \theta), \quad (19)$$

where  $\phi_k \sim p(\phi)$ . In practice this approach tends to underestimate  $\mathcal{L}$ .

**Lower bound on the log-expectation** The intractable log-likelihood  $\mathcal{L}$  can be approximated in multiple ways. We can simply estimate the biased Jensen posterior by moving the logarithm inside the integral (Wenzel et al., 2020):

$$\log p(\mathcal{D}|\theta) = \sum_{n=1}^N \log \int p(\mathbf{y}_n|\mathbf{x}_n, \phi; \theta) p(\phi) d\phi \quad (20)$$

$$\geq \sum_{n=1}^N \int \log p(\mathbf{y}_n|\mathbf{x}_n, \phi_k; \theta) p(\phi) d\phi \quad (21)$$

$$\approx \sum_{n=1}^N \frac{1}{K} \sum_{k=1}^K \log p(\mathbf{y}_n|\mathbf{x}_n, \phi_k; \theta), \quad (22)$$

where  $\phi_k \sim p(\phi)$ . This represents a lower bound of the true augmented likelihood, for which Monte-Carlo approximation is unbiased. The Jensen bound can be applied with importance sampling to tighten the bound (Burda et al., 2016; Luo et al., 2020).

**Bias correction** We can also apply a bias-correction (Durbin and Koopman, 1997; Shephard and Pitt, 1997) to the sample mean of  $\exp(\mathcal{L})$ . First, we imagine wanting to estimate the logarithm of an integral  $I$ , considering a Monte Carlo approximation of the integral  $I$  itself,

$$I = \int p(\mathbf{y}|\mathbf{x}, \phi, \theta) p(\phi) d\phi \quad (23)$$

$$I \approx I_K = \frac{1}{K} \sum_k p(\mathbf{y}|\phi_k, \mathbf{x}, \theta), \quad \phi_k \sim p(\phi). \quad (24)$$

It can be shown that the estimator  $I_K$  can be turned into an unbiased estimator as follows (Durbin and Koopman, 1997; Shephard and Pitt, 1997)

$$\log I \approx \log I_K + \frac{1}{2} \frac{\text{var}[I_K]}{I_K^2} \quad (25)$$

$$\text{var}[I_K] = \frac{1}{K(K-1)} \sum_k (p(\mathbf{y}|\mathbf{x}, \phi_k, \theta) - I_K)^2 \quad (26)$$

$$0 = \mathbb{E} \left[ \log I_K + \frac{1}{2} \frac{\text{var}[I_K]}{I_K^2} \right]. \quad (27)$$

The correction makes the log-integral unbiased with respect to different samplings  $(\phi_1, \dots, \phi_K) \sim p(\phi)$ . With  $K = 1$  the approximation the log-integral is already unbiased, but it suffers from large variance. In image classification,  $K$  refers to the number of corruptions per image within a mini-batch. The correction is most beneficial in small- $K$  regimes. For instance, in Batch Augmentation multiple instances of each image are used within a batch (Hoffer et al., 2020).

**Tempering vs augmented likelihood** Our marginalized additive augmented likelihood Eq. 17 aligns with the ‘Jensen’ likelihoods discussed by [Wenzel et al. \(2020\)](#). In contrast, [Kapoor et al. \(2022\)](#) argues for multiplicative tempered augmented likelihood

$$p_{\text{geom}}(\mathcal{D}|\theta) = \prod_{n=1}^N \prod_{k=1}^K p(\mathbf{y}_n|\mathbf{x}_n, \phi, \theta)^{1/K}, \quad (28)$$

where the augmentations are aggregated by a geometric mean. These approaches are connected: the geometric likelihood Eq. 28 is the lower bound Eq. 21 of the augmented likelihood Eq. 20. In the geometric likelihood we can interpret the augmentations as down-weighted data points, which are assumed to factorize despite not being i.i.d.. In the augmented likelihood we interpret the data points as i.i.d. samples, and augmentations as expanding each sample into a distribution, which leads to a product over observations and integral over augmentations.